A combined theoretical and experimental study of the valence and Rydberg states of iodopentafluorobenzene

Michael H. Palmer, Søren Vrønning Hoffmann, Nykola C. Jones, Marcello Coreno, Monica de Simone, Cesare Grazioli, Kirk A. Peterson, Alberto Baiardi, Teng Zhang, and Malgorzata Biczysko

Citation: The Journal of Chemical Physics **146**, 174301 (2017); doi: 10.1063/1.4981919
View online: http://dx.doi.org/10.1063/1.4981919
View Table of Contents: http://aip.scitation.org/toc/jcp/146/17
Published by the American Institute of Physics

A combined theoretical and experimental study of the valence and Rydberg states of iodopentafluorobenzene

Michael H. Palmer,[1,a)] Søren Vrønning Hoffmann,[2,b)] Nykola C. Jones,[2,b)] Marcello Coreno,[3,b)] Monica de Simone,[4,b)] Cesare Grazioli,[3,b)] Kirk A. Peterson,[5,b)] Alberto Baiardi,[6,b)] Teng Zhang,[7,b)] and Malgorzata Biczysko[8,b)]

[1]*School of Chemistry, University of Edinburgh, Joseph Black Building, David Brewster Road, Edinburgh, EH9 3FJ Scotland, United Kingdom*
[2]*ISA, Department of Physics and Astronomy, Aarhus University, Ny Munkegade 120, DK-8000 Aarhus C, Denmark*
[3]*CNR-ISM, Trieste LD2 Unit, 34149 Trieste, Italy*
[4]*CNR-IOM Laboratorio TASC, 34149 Trieste, Italy*
[5]*Department of Chemistry, Washington State University, Pullman, Washington 99164-4630, USA*
[6]*Scuola Normale Superiore, Piazza Cavalieri 7, 56126 Pisa, Italy*
[7]*Department of Physics and Astronomy, University of Uppsala, Uppsala, Sweden*
[8]*International Centre for Quantum and Molecular Structures, College of Sciences, Shanghai University, 99 Shangda Road, Shanghai 200444, China*

(Received 20 February 2017; accepted 10 April 2017; published online 1 May 2017)

A new ultraviolet (UV) and vacuum ultraviolet (VUV) spectrum for iodopentafluorobenzene (C_6F_5I) using synchrotron radiation is reported. The measurements have been combined with those from a recent high-resolution photoelectron spectroscopic study. A major theoretical study, which includes both Franck-Condon (FC) and Herzberg-Teller (HT) analyses, leads to conclusions, which are compatible with both experimental studies. Our observation that the VUV multiplet at 7.926 eV in the VUV spectrum is a Rydberg state rather than a valence state leads to a fundamental reassignment of the VUV Rydberg spectrum over previous studies and removes an anomaly where some previously assigned Rydberg states were to optically forbidden states. Adiabatic excitation energies (AEEs) were determined from equations-of-motion coupled cluster with singles and doubles excitation; these were combined with time dependent density functional theoretical methods. Frequencies from these two methods are very similar, and this enabled the evaluation of both FC and HT contributions in the lower valence states. Multi-reference multi-root configuration interaction gave a satisfactory account of the principal UV+VUV spectral profile of C_6F_5I, with vertical band positions and intensities. The UV spectral onset consists of two very weak transitions assigned to 1^1B_1 ($\pi\sigma^*$) and 1^1B_2 ($\sigma\sigma^*$) symmetries. The lowest unoccupied molecular orbital of a $\sigma^*(a_1)$ symmetry has a significant C–I* antibonding character. This results in considerable lengthening of the C–I bond for both these excited states. The vibrational intensity of the lowest 1^1B_1 state is dominated by HT contributions; the 1^1B_2 state contains both HT and FC contributions; the third band, which contains three states, two $\pi\pi^*(1^1A_1, 2^1B_2)$ and one $\pi\sigma^*(2^1B_1)$, is dominated by FC contributions in the $^1A_1$ state. In this $^1A_1$ state, and the spectrally dominant bands near 6.7 ($^1A_1$) and 7.3 eV ($^1A_1 + {}^1B_2$), the C–I bond length is in the normal range, and FC components dominate. *Published by AIP Publishing.* [http://dx.doi.org/10.1063/1.4981919]

I. INTRODUCTION

Interpretation of the photoelectron spectroscopic (PES)[1] and vacuum ultraviolet (VUV) spectra[2] of iodobenzene (C_6H_5I) was simplified by parallel studies using the two methods. Recently, we reported a new high-resolution PES spectrum of iodopentafluorobenzene (C_6F_5I),[3] which showed substantially improved vibrational resolution over the previous study.[4]

The present paper contains a new synchrotron based investigation of the VUV spectrum of C_6F_5I. The necessity for this arose from previous assignments of Rydberg states in the VUV spectrum to optically forbidden states.[4] In our theoretical analysis, we investigate the VUV spectrum with high level theoretical studies. These include both Franck-Condon (FC) and Herzberg-Teller (HT) analyses of the vibrational structure.[5–9] This combination of theory with experimental PES and VUV spectra allows a more reliable interpretation of the VUV region.

The similarity between the VUV spectra of C_6H_5I and C_6F_5I, demonstrated in Fig. 1, is discussed below. We adopt the VUV band identities used by Eden *et al.*[4] (A to F) for convenience in comparisons and extend it to higher energies. There are a significant number of studies of the photochemistry of C_6F_5I. Since we are considering the static spectral

[a)]Author to whom correspondence should be addressed. Electronic mail: m.h.palmer@ed.ac.uk. Telephone: +44 (0) 131 650 4765.
[b)]Electronic addresses: vronning@phys.au.dk; nykj@phys.au.dk; marcello.coreno@elettra.eu; desimone@iom.cnr.it; kipeters@wsu.edu; cesare.grazioli@elettra.eu; alberto.baiardi@sns.it; teng.zhang@physics.uu.se; and biczysko@shu.edu.cn.

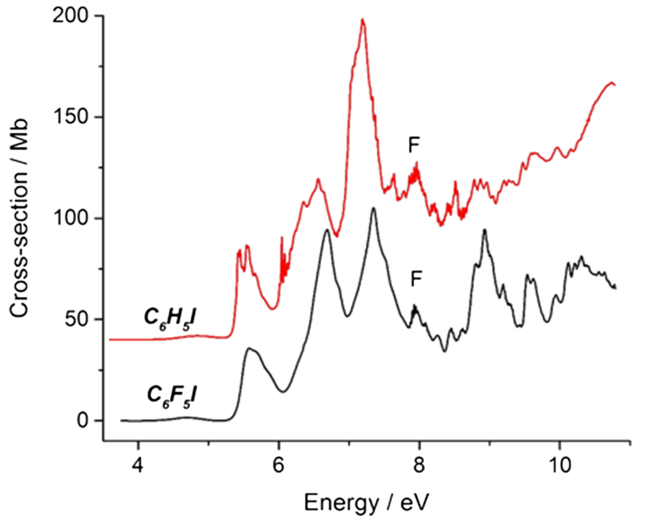

FIG. 1. UV+VUV spectra of C_6F_5I and C_6H_5I, which demonstrate the considerable spectral similarity between the two molecules. The region marked "F" is crucial to the assignment of Rydberg states for both molecules and is discussed in the text. The baseline of the C_6H_5I spectrum is raised to improve the clarity.

properties of C_6F_5I, many dynamic photochemical studies are unimportant, but the nature of under-lying states during irradiation is important. Most earlier photochemical and UV+VUV studies used wavelength units (nm). Here we need to compare with ionization energies from the PES study, usually expressed in electron volts (eV). Similarly, the vibrational splitting for Rydberg states is given in cm^{-1}. We use both nm and eV in the Introduction, but in Sections II–IV we will use eV for broad ranges and cm^{-1} for vibrations.

In the photochemistry of aryl iodides,[10–14] the terms "bands A, B, and C" have a different meaning, and where necessary these are shown in parentheses. The notation for the photochemical "band A" arises from comparison with alkyl halide absorption (e.g., CH_3I). For C_6F_5I, this lies between ~200 and 350 nm (6.20 to 3.54 eV). These transitions involve promotion of an I (5*p*) non-bonding electron to an antibonding σ* orbital centred on the C–I bond. Irradiation in that range causes rapid photo-dissociation, liberating both I ($^2P_{3/2}$) and I* ($^2P_{1/2}$). Although a similar process occurs with aryl iodides, e.g., C_6F_5I and C_6H_5I,[2] the presence of π + σ doubly occupied molecular orbitals (DOMOs) and low-lying π* and σ* virtual molecular orbitals (VMOs) makes the situation more complex, as is discussed further below. Perfluoro compounds, such as C_6F_5I and C_6F_5H, when compared with the corresponding perhydro compounds, C_6H_5I and C_6H_6, show an energy lowering for both *occupied MOs and virtual MOs*. Thus πσ* transitions become more probable.[10,11] Kavita and Das[12] used a range of dissociation wavelengths from 222 to 305 nm (5.58 to 4.06 eV), and proposed that photochemical excitation leads to a charge-transfer ππ* state. Griffiths *et al.*[13] studied the energetics of I liberation from C_6F_5I, by separate irradiation at 304.67 nm (4.069 eV) and 304.02 nm (4.078 eV), enabling both I and I* to be identified. Similar results were obtained with irradiation of C_6H_5I at 304.7 nm, where the I release was attributed to both ^{3}nσ* and ^{3}ππ* state intermediaries.[14] These energies are close to the onset of UV absorption by C_6F_5I, which contains the two states, $^1B_1$ ($\pi\sigma^*$, $6b_1 13a_1^*$) and $^1B_2$ ($\sigma\sigma^*$, $11b_2 13a_1^*$) previously mentioned.

Complete active space self-consistent field (SCF, CASSCF) calculations, including spin-orbit coupling, have put these photochemical effects on a more rigorous basis.[15,16] Ajitha *et al.*[15] compared transitions of alkyl iodides (CX_3I) with C_6X_5I and C_6X_5H, where X = H and F. Several low-lying *n*σ*, ππ*, and πσ* transitions were identified, although the picture was incomplete for C_6F_5I. Murdock *et al.*[16] unified the excitation description for both alkyl and aryl iodide photochemistry. Promotion of an I (5p) non-bonding electron, to a σ* orbital localized on the C–I bond, results in a rapid bond cleavage. Spin-orbit coupling splits this excitation into three overlapping *n*σ* absorption continua, labelled in Mulliken notation as $^1Q_1$, $^3Q_1$, and $^3Q_{0+}$. Excitation to the *n*σ* ($^3Q_{0+}$) state, followed by direct dissociation, yields the spin-orbit excited iodine atom (I*) product. Non-adiabatic coupling via a conical intersection (ConInt) with the $^1Q_1$ potential yields the ground state iodine I atoms. These conclusions provide a good model for aryl iodide photochemistry.[16]

Our current objective is to re-interpret the VUV spectrum of C_6F_5I in the light of both our recent investigation of the PES for the compound[3] and theoretical methods. We hope to correlate the results with those for both C_6H_5I and C_6F_5H.

The study will include the determination of adiabatic excitation energies (AEE) for some singlet states in the UV+VUV spectrum, by the use of time-dependent density functional theoretical (TDDFT) methods.[17,18] The onset of the UV bands for C_6F_5I is very weak; the experimental AEEs are difficult to identify and cannot readily be compared with the theoretical AEE. A more realistic comparison between results of the theoretical study and experiment is to compare the vertical excitation energies (VEEs) with spectral band maxima, which are more distinct. However, these observed maxima may only be the summation of vibrational effects and not refer to a discrete electronic state.

We use the multi-reference multi-root configuration interaction (MRD-CI) study[19] for the VEE. A set of reference configurations are expanded to include all single and double excited configurations; the resultant secular equations are diagonalised to generate energy solutions (roots) for the excited states, as described in our previous papers.[1–3] Additional results are deferred to the supplementary material as SM1.

II. SPECTROSCOPIC AND THEORETICAL METHODS

A. Experimental VUV spectroscopy

The VUV absorption spectrum for C_6F_5I, recorded at room temperature, was measured on the AU-UV beam line of the ASTRID2 storage ring (Aarhus University, Denmark); the experimental setup has been described in detail previously.[2] The spectral energy range was from 3.757 eV (330 nm, 30 300 cm^{-1}) to 10.781 eV (115 nm, 86 954 cm^{-1}). The data points (total 2426) had separations ranging from 0.02 to 0.2 nm over this spectral region. The MRD-CI[19] calculated VEEs and oscillator strengths (f(r)) are superimposed on the VUV spectrum in Fig. 2. Colour coding shows the symmetries of the allowed states. Generally, there is a reasonable

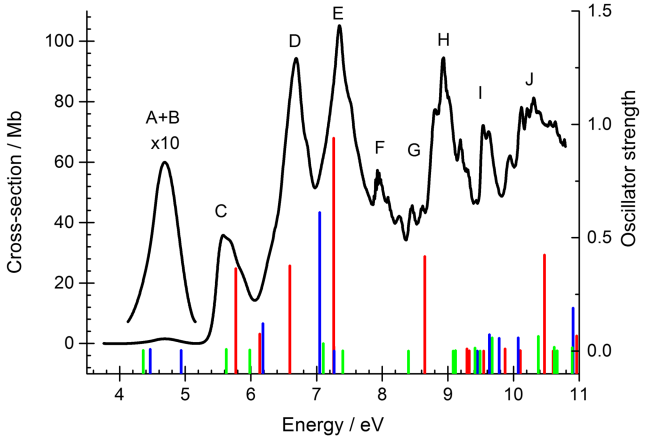

FIG. 2. The C_6F_5I vacuum ultraviolet spectrum with calculated MRDCI singlet state values. The excited states are coloured $^1A_1$ (red), $^1B_2$ (blue), and $^1B_1$ (green). $^1A_1$ states are dominant; $^1A_2$ states are omitted. The principal regions are labelled following Eden *et al.*,[3] and extended to higher energies.

correlation between the theory and experiment, as discussed below.

B. Computational procedures

No single computational chemistry package offers all the facilities required. Modules from each of CFOUR[20] (AEE, equilibrium structures at the equations-of-motion coupled cluster with singles and doubles excitation (EOM-CCSD) level,[21] and harmonic frequencies) GAUSSIAN-09[22] (G-09, TDDFT studies and vibrational analyses using FC and HT methods[5–9]), and GAMESS-UK[23] (MRD-CI studies) were utilised.

Basis sets used in the EOM-CCSD study took into account the relative polarities of the atoms as follows: C atoms were represented by correlation consistent double (T) zeta valence + polarization basis sets (cc-pVDZ);[24] F atoms by augmented versions (aug-cc-pVDZ); I atom by aug-cc-pVDZ-PP, respectively.[25] The I atom basis included a 28-electron scalar relativistic effective core potential (ECP). This last basis set was used for comparisons between molecules as discussed below. The TDDFT calculations employed contracted [3s3p1d] LANL2DZdp[26] sets for C and F with the uncontracted (3s4p1d) LANL08d set for iodine.[27] The latter includes a large-core, 46-electron ECP, which includes mass-velocity and Darwin relativistic effects.[28] The DFT functional was B3LYP.[29] The TDDFT method is limited to single excitation CI.

The X^1A_1 ground state of C_6F_5I contains 67 doubly occupied MOs (DOMOs) when using all-electron (AE) bases. All 34 core orbitals were frozen in the CI calculations. The resultant valence shell contains 33 DOMOs ($13a_1$, $6b_1$, $11b_2$, $3a_2$), and we use this numbering throughout. Up to 104 virtual molecular orbitals (VMOs) were included in the MRD-CI study.

There is a paucity of structural data for C_6F_5I. The only experimental structure for C_6F_5I is derived from ^{13}C satellites in its ^{19}F NMR spectrum.[30] The present X^1A_1 ring structure is relatively close to this, as shown in the supplementary material as SM2. Covalent atomic radii for C (sp^2), F, and I (0.73, 0.64, 1.33 Å, respectively)[31,32] suggest that some degree of steric congestion occurs around C_1 in this structure. Lengthening of the C–I bond in some excited states, and facile release of the I atom in photochemistry, may be a result of this. We observed that the ring retains the C_{2V} symmetry for excited states with a lengthened C–I bond, but where a C–I shortening occurs, slight ring buckling along the C_1C_4 axis to C_S symmetry also occurs; however, we retain the C_{2V} labelling here. In this distorted state, downward folding of C_2C_3/C_5C_6 of the ring enables the I atom to tilt above the C_1C_4 axis.

III. RESULTS AND DISCUSSION

A. General points

In our theoretical analysis, all structures and derived information, such as MO electron density plots, harmonic frequencies, Franck-Condon (FC) factors, and Herzberg-Teller (HT) effects, relate to the equilibrium structure of the state in question. Similarly, computational AEE and VEE energy results are with respect to the X^1A_1 state at the equilibrium geometry, using the same theoretical procedure.

Singlet state structures were determined by EOM-CCSD procedures.[17] Structural variations between electronic states were found to be similar to the TDDFT calculations; comparisons are shown in the supplementary material as SM2, since excited state structures are not important to the main focus of this paper. The principal low-lying and high intensity electronic states are listed in Table I. Under C_{2v} constraints, the EOM-CCSD and TDDFT harmonic vibration frequencies (VibFreq) are remarkably similar, and allowed linear correlations for each state to be performed. This provided a solution to the observation that the EOM-CCSD method generates two imaginary frequencies (modes 19 and 20 both for the b_1 symmetry) for the 1^1A_1 state, whereas the TDDFT 1^1A_1 state generates a single imaginary frequency, and otherwise has very similar numerical values. The FC software[5–9] in G-09[22] only allows the projection out of a single imaginary frequency (IF) and also does not perform the HT vibrational analysis at the EOM-CCSD level. Substitution of the linear correlation TDDFT values for EOM-CCSD values allowed the FC analyses to be performed. The harmonic frequencies in Table II are EOM-CCSD for each of the X^1A_1, $^1B_1$, and $^1B_2$ excited states; the 1^1A_1 state values are from the linear correlation with the TDDFT results.

Although such IF are indicative of a saddle point rather than a genuine minimum, for the EOM-CCSD 1^1A_1 structure, the implicit distortions from C_{2V} must be small, since the TDDFT method gave one IF. More information is given in the supplementary material under SM2, but the correlation procedure was performed separately for each state; the slope obtained in each case was used to "scale" the TDDFT results, which were then inserted into the FC + HT analyses.

B. The valence shell MOs of highest importance to the singlet and triplet state excitations of C_6F_5I (C_{2v})

Using the X^1A_1 ground state structure, the CI, EOM-CCSD, and TDDFT calculations all show that the low-lying

TABLE I. Selected VEE valence states calculated by the MRD-CI method. Typical values of the second moments show the difference between valence and Rydberg states, indicated by capital S, for two Rydberg s-states.

Energy (eV)	Oscillator strength/f(r)	Symmetry	Leading configuration	$\langle x^2 \rangle$ a.u.^{2}	$\langle y^2 \rangle$ a.u.^{2}	$\langle z^2 \rangle$ a.u.^{2}
0	0	$^1A_1$	X^1A_1	−64	−70	−66
4.360	0.002 318	$^1B_1$	$6b_1 14a_1$*	−62	−69	−70
4.466	0.007 826	$^1B_2$	$8b_2 14a_1$*	−66	−70	−72
4.937	0.002 906	$^1B_2$	$3a_2 7b_1$*	−64	−69	−65
5.624	0.007 815	$^1B_1$	$5b_1 14a_1$*	−66	−70	−83
5.748	0.377 849	$^1A_1$	$6b_1 7b_1$*	−63	−70	−62
5.982	0.005 049	$^1B_1$	$11b_2 4a_2$*	−62	−69	−71
6.593	0.375 456	$^1A_1$	$3a_2 4a_2$*	−63	−69	−65
7.261	0.938 907	$^1A_1$	$5b_1 7b_1$*	−63	−69	−63
7.344	0.610 940	$^1B_2$	$6b_1 4a_2$*	−63	−70	−62
7.102	0.000 209	$^1B_1$	$6b_1$S	−188	−195	−196
7.201	0.014 597	$^1B_2$	$8b_2$S	−187	−191	−189

excited states of C_6F_5I in Fig. 3 are dominated by the group of highest occupied MOs (HOMOs) and lowest unoccupied MOs (LUMOs, also known as virtual molecular orbitals, VMOs). The MOs featured in Fig. 3 are the only ones which are heavily populated in the excited states discussed in this paper. Higher VMOs are likely to be involved in higher electronic states, but these may well be distorted by the presence of Rydberg states.

TABLE II. The unscaled EOM-CCSD harmonic vibration frequencies (cm^{-1}) for low-lying singlet states. Two imaginary frequencies are marked "*i*." The corresponding TDDFT values contain only one imaginary frequency.

Mode	Symmetry	X^1A_1	1^1B_1	1^1B_2	1^1A_1
1	a_1	1710	1675	1683	1744
2	a_1	1567	1547	1548	1458
3	a_1	1453	1419	1435	1337
4	a_1	1284	1251	1253	1259
5	a_1	1091	1054	1052	1051
6	a_1	809	689	697	822
7	a_1	580	575	575	559
8	a_1	494	469	470	462
9	a_1	356	330	330	337
10	a_1	280	270	268	268
11	a_1	205	89	89	206
12	a_2	671	670	670	550
13	a_2	405	401	401	212
14	a_2	133	126	129	121
15	b_1	662	671	669	464
16	b_1	635	605	597	311
17	b_1	364	341	337	182
18	b_1	216	212	208	156
19	b_1	167	160	161	−84i
20	b_1	81	30	34	−359i
21	b_2	1701	1972	1715	1628
22	b_2	1553	1543	1547	1384
23	b_2	1268	1281	1283	1271
24	b_2	1155	1140	1138	1023
25	b_2	987	968	969	919
26	b_2	747	715	720	721
27	b_2	444	484	434	442
28	b_2	310	299	302	303
29	b_2	274	279	274	268
30	b_2	130	49	33	138

None of these MOs is rich in F atom density, since this occurs in more tightly bound MOs.

A comparison of the spatial composition of the LUMOs between C_6H_5I[1,2] and those for C_6F_5I (in Fig. 3) shows strong electron density similarities, but the symmetry sequence is different. Since similarities and differences occur in both the HOMO and LUMO sets, we can expect that these will be reflected in the experimental VUV spectra, and this is demonstrated in Fig. 1.

The considerably different number of valence DOMOs between the two molecules makes comparisons by symmetry the most appropriate. In more detail, we show a correlation diagram (Fig. 4) of the highest group of MOs for C_6H_6, C_6H_5I, C_6F_5I, and C_6F_5H. These MOs are closely related to those of Fig. 3; all molecules are at their equilibrium structures, and all were determined using the same basis sets and theoretical method Roothaan-Hartree-Fock (RHF).

After taking account of the D_{6H} to C_{2V} changes, there is a considerable similarity between the group of C_{2V} orbitals correlating with the π-MOs ($1e_{1g}$ and $1a_{2u}$) and highest σ-MO ($3e_{2g}$) of benzene. These states are clearly visible in the PES of C_6H_6 and are established in energy as $1e_{1g}{}^{-1} < 3e_{2g}{}^{-1} < 1a_{2u}{}^{-1}$ ionizations. Thus, $1e_{1g}$ splits under C_{2V} conditions into b_1 and a_2 π-MO components, with $3e_{2g}$ becoming a_1 and b_2 σ-MOs. The introduction of the I-atom inserts additional lone-pair orbitals into the correlation, with the effect of the C–I σ-MO lying at higher energy. The major effects of the F-atom electrons also lie at higher energies, but clear demonstration of the relatively small "perfluoro-effect" can be seen by the lowering of the π-orbital energies close to 1.0 eV. The inner π-MO, $1a_{2u}$ of benzene, is shifted across the series by a similar amount, on F-substitution. A more dramatic effect lies on the σ-MOs, where the steeper lowering of energy is close to 2 eV for the $3e_{2g}$ σ-MO. Thus, although the F-atoms are π-donors to the ring, the most important effect is σ-withdrawal from the ring. The F-atom electronegativity effect shows as the smaller (second order) effect, by tightening the σ-bonding and lowering of the energy of the MOs.

In the X^1A_1 ground states, the LUMO for C_6F_5I is a σ*-MO ($14a_1$*) which contrasts with a π*-LUMO ($7b_1$*) for C_6H_5I. However, this sequence changes when electrons are

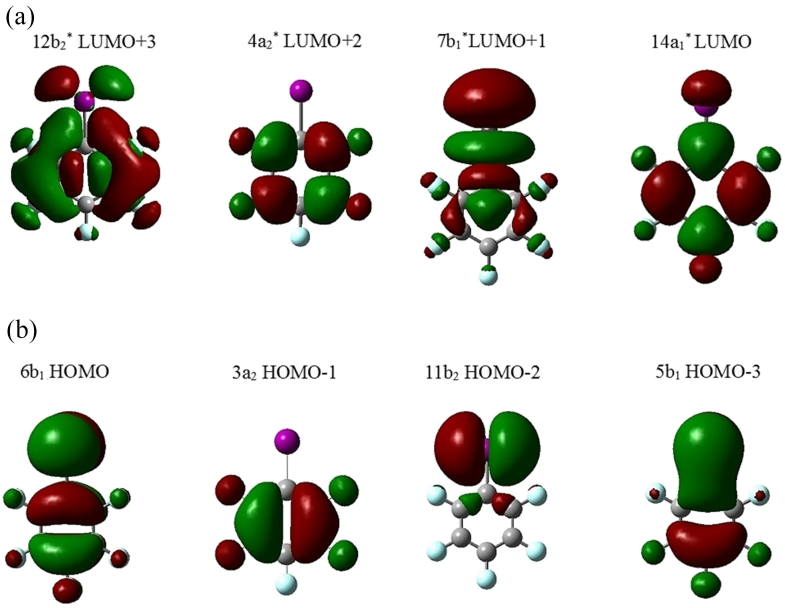

FIG. 3. Constant density (0.02e) MO contour diagrams of C_6F_5I. (a) The lowest valence unoccupied (virtual) MOs of each symmetry; these are occupied in the lower singlet valence excited states. (b) The four highest occupied MOs (HOMOs) using valence shell numbering (67 occupied MOs reduced to 28 MOs); when ionized the sequence remains as $6b_1^{-1} < 3a_2^{-1} < 11b_2^{-1} < 5b_1^{-1}$; these are the X, A, B, and C states, respectively.

promoted to occupy these LUMOs. The lowest excited states for C_6H_5I occur in the same sequence as for C_6F_5I. These σ-LUMOs are involved in several of the lowest excited states of both C_6H_5I and C_6F_5I. The two lowest singlet states are $\pi\sigma^*$ (1^1B_1) and $\sigma\sigma^*$ (1^1B_2), respectively, for both. The C–I anti-bonding character introduced by an occupancy of $14a_1$* results in a very long C–I bond.

The second moments (SecMom) of the charge distribution ($\langle x^2\rangle$, $\langle y^2\rangle$, and $\langle z^2\rangle$) as well as excitation energy data are shown in Table I. The clear distinction between MOs for valence and Rydberg states is given by the SecMom; the two Rydberg states have very much larger values. Conversely, a Rydberg upper state MO would show a very low electron density in the region close to the nuclei, and little density would be shown relative to the orbitals in Fig. 3. This is in strict contrast to the density in $14a_1$*, a valence state.

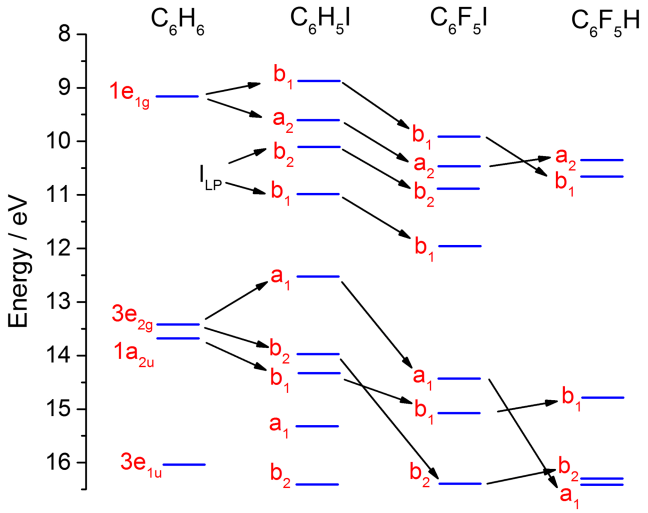

FIG. 4. The highest sequence of occupied MOs for benzene, iodobenzene, iodopentafluorobenzene, and pentafluorobenzene at their corresponding equilibrium structures. The correlations shown are relevant to the perfluoro-effect, where small shifts are both predicted for π-ionizations, with larger effects for σ-ionizations. These are observed in photoelectron spectra in favourable cases.

C. Analysis of the UV+VUV absorption spectrum for C_6F_5I and its theoretical interpretation

Our new experimental UV+VUV absorption spectrum of C_6F_5I is shown in Figs. 1 and 2 (black trace), with the lowest absorption region shown as a 10 times expansion. At this level of detail, it does not differ from the previous spectrum.[4] We retain the Eden *et al.*[4] spectral band labelling (A–F) but comment that several of their assignments are revised below. A detailed analysis of the vibrational structure of the observed bands is performed by both Franck-Condon (FC) factor and Herzberg-Teller (HT) analyses of some electronic states, as shown below.

The earliest UV+VUV study[33] of C_6F_5I in the spectral energy range 4.5 to 9.5 eV compared three singlet states with those of benzene ($^1B_{2u}$, $^1B_{1u}$, and $^1E_{1u}$)[34] and with related fluorobenzenes ($C_6F_nH_{6-n}$). In contrast, Eden *et al.*[4] compared their valence states with electronic states observed for C_6F_5Br and C_6F_6. The closest correlation is of C_6F_5I with C_6H_5I, where we have recently reported a detailed analysis;[1,2] this comparison is described below.

D. Valence states

We believe that the principal regions where valence states occur in the experimental UV+VUV spectrum are near 4.7, 5.6, 6.8, and 7.3 eV; most of the structures elsewhere in the UV+VUV spectrum are Rydberg in nature, which is discussed below.

The lowest lying spectral states have a very low intensity, making the actual onset difficult to determine and comparison with calculated AEE impossible. Comparison of the observed and calculated VEEs is more appropriate. Singlet state VEEs with oscillator strengths (f(r)), colour coded by symmetry, are super-imposed on Fig. 2. The MRD-CI method used includes numerous configuration state functions (CSFs) which represent all possible $\pi\pi^*$, $\sigma\sigma^*$, $\sigma\pi^*$, and $\pi\sigma^*$ excitations, using a singles + doubles CI method. In this method, an initial set of assumed CSFs is increased until the output wave function shows no further CSF appearing; this process

leads to the highest possible level of electron correlation. These MRD-CI calculations give a reasonable interpretation of the observed VUV spectrum in terms of principal band maxima (Fig. 2). The low energy states and others with strong oscillator strength in the VUV are shown in Table I. $^1A_1$ states are clearly dominant in intensity. All these calculated VEE results were determined at the X^1A_1 ground state structure. An extended table of VEE and f(r) appears in the supplementary material as SM2.

Although Rydberg states are discussed in detail at a later stage, two calculated Rydberg states are included in Table I for spatial comparison with valence states. In the Rydberg state calculations, the basis set includes both valence and very diffuse functions (exponents <0.01). A variety of calculated valence and Rydberg states are generated within this same multi-root CI. Our theoretical study basis sets show whether a calculated state is of valence or Rydberg type, by means of the second moments of the charge distribution ($\langle x^2\rangle$, $\langle y^2\rangle$, and $\langle z^2\rangle$). Those shown in Table I give a quantitative measure of the level of the diffuse character in an electronic state. States with terms similar to those of the electronic X^1A_1 ground state are valence in character. Rydberg states, where the upper state electron is generally far from the nuclei, have high $\langle x^2\rangle$ through the diffuse character.

An early requirement was to determine the FC and HT components of intensity for the lowest observed UV bands. The lowest group of calculated AEEs involves excitation into the LUMO ($14a_1$*, Table I) from each of the DOMOs, $6b_1$, $5b_1$, $3a_2$, and $8b_2$. The TDDFT method using our standard all-electron basis sets gave a very low AEE, while the structures showed long C–I bond lengths (2.5 to 2.75 Å). However, a similar behaviour over the C–I bond lengths also occurred in the EOM-CCSD calculations, and we conclude that these extensions to that bond are realistic.

1. The experimental spectral onset region below 5.2 eV (42 000 cm^{-1})

Strong similarities between the spectra of C_6H_5I and C_6F_5I are apparent in Fig. 1. For C_6F_5I, a very weak maximum occurs at 37 808 cm^{-1} (4.688 eV); the cross section at 30 300 cm^{-1} (3.757 eV) is 0.03 Mb and must lie close to the spectral onset. This band is asymmetric, with a slow onset, consistent with the presence of more than one state.

The two low-lying singlet states, $^1B_1$ ($6b_1 14a_1$*) and $^1B_2$ ($8b_2 14a_1$*), under the envelope in this spectral region, both involve excitation into the $14a_1$* LUMO, as shown in Fig. 3 and Table I. These states have TDDFT calculated 0–0 bands at 33 140 (1^1B_1) and 34 404 (1^1B_2) cm^{-1}, respectively. The EOM-CCSD 0–0 separation of states is only 140 cm^{-1}. Since this would lead to a loss of clarity in Fig. 4, the bands are separated at the TDDFT separation. This is consistent with the bands labelled A + B by Eden *et al.*[4] Previous cases of low-lying πσ* and σσ* states are known for fluorinated benzenes.[10,11]

We show these two theoretical 1^1B_1 and 1^1B_2 states for C_6F_5I in Fig. 5. Both states show the dominant single vibrational progressions, as in Tables III and IV. The intensities shown here represent the total of both FC and HT contributions, which vary considerably. The 1^1B_1 state contains over 85% HT contribution (Table III). The 1^1B_2 state shows less HT components, but is still greater than 55% (Table III). The HT proportion possibly increases with the sum of the vibration frequency combinations involved. The ratio of the intensities of the Franck-Condon (FC) to Herzberg-Teller (HT) contributions, is markedly different between the $^1B_2$ and $^1B_1$ states, with HT/FC being 6.6 and 1.5 respectively.

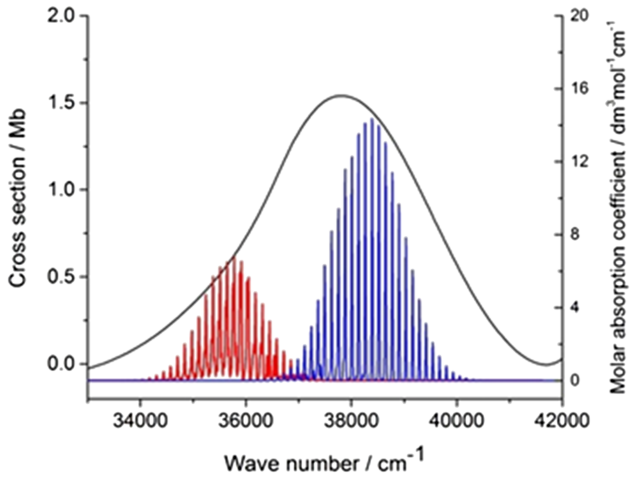

FIG. 5. The onset region of the UV spectrum for C_6F_5I. The combined vibrational profiles for the Franck-Condon and Herzberg-Teller cold bands are inset for the $^1B_1$ (red) and $^1B_2$ states (blue). The combined theoretical spectra have been shifted to overlay the observed spectral band. The relative positions of the two states are at the TDDFT theoretical difference; the EOM-CCSD energy difference is much smaller at 140 cm^{-1}, which would not allow the present simplicity.

The main progression for 1^1B_1 is 11^N where the maximum occurs when N, as in Tables III and IV, the number of quanta excited, is 31 for the spectrum shown in Fig. 5. This is consistent with considerable lengthening of the C–I bond in the 1^1B_1 state (2.535 Å) relative to the X^1A_1 state (2.089 Å). The splitting on the high-energy side of 1^1B_1 arises from two simultaneously excited modes of 11^N with each of 10^1, 9^1, 8^1, and 6^1. Combination bands including 7^1 have significantly lower intensity. Under the Herzberg-Teller analysis, the lowest vibrational contributions arise from mode 11^N with each of the b_1 modes, 17, 16, and 15.

The main FC progression for 1^1B_2 is again 11^N with maximum intensity when N is 39; the considerable lengthening of the C–I bond in this state (2.635 Å) relative to the ground state is again consistent with this. No other calculated vibrational sequences, in either FC or HT analyses, for this state have a significant intensity.

2. The region between 5.5 and 6 eV (band C)

Many benzene derivatives have an absorption band in this energy range,[33,34] which relates to the $^1B_{2u}$ state of the parent molecule. The present example shows a less vibrational structure than that for C_6H_5I (Fig. 1). One potential reason is the overlap of excited states, since our study suggests that three singlet states occur here (Fig. 2). The dominant state (Table I) of $^1A_1$ ($6b_1 7b_1$*) symmetry is accompanied by two $^1B_1$ states

TABLE III. Selected intensities for the Franck-Condon (FC) and Herzberg-Teller (HT) factors for some low-lying singlet states; these are cold bands only, based on harmonic vibration frequencies. In order to allow processing of Herzberg-Teller contributions, the EOM-CCSD were correlated to the TDDFT values, which led to the removal of one imaginary frequency. The frequencies shown here are based upon that correlation. See the supplementary material for additional details.

Vibrational state	Frequency (cm^{-1})	Intensity			
		Franck-Condon	Herzberg-Teller	Total	HT (%)
(a) The $^1B_1$ state: energy of the 0–0 transition: 33 140 cm^{-1}					
11^{26}	3328	3.4	20.2	23.6	86
$17^1 11^{24}$	3438	...	6.3	6.3	
11^{27}	3456	4.6	27.9	32.4	86
$8^1 11^{24}$	3560	1.0	6.5	7.6	86
$17^1 11^{25}$	3566	...	10.5	10.5	
11^{28}	3584	3.8	23.6	27.4	86
$17^1 11^{26}$	3694	...	15.7	15.7	
11^{29}	3712	5.1	32.7	37.8	86
$10^1 11^{27}$	3742	1.3	8.5	9.7	87
$9^1 11^{27}$	3808	1.3	9.2	10.6	87
$17^1 11^{27}$	3822	...	20.9	20.9	
11^{30}	3840	6.2	40.4	46.6	87
$10^1 11^{28}$	3840	1.7	11.5	13.2	87
$9^1 11^{28}$	3936	1.1	7.4	8.5	88
$8^1 11^{27}$	3944	3.3	21.8	25.1	87
$17^1 11^{28}$	3950	...	18.1	18.1	
11^{31}	3968	6.7	44.8	51.5	87
$16^1 11^{26}$	3982	...	19.1	19.1	
$10^1 11^{29}$	3998	2.0	14.0	16.1	87
$9^1 11^{29}$	4064	1.4	10.0	11.4	88
$6^1 11^{26}$	4069	1.3	9.4	10.6	88
$17^1 11^{29}$	4078	...	24.1	24.1	
11^{32}	4092	4.5	30.9	35.4	87
11^{33}	4224	4.9	34.4	39.3	88
11^{34}	4352	4.8	34.3	39.0	88
$15^1 11^{28}$	4404	...	13.2	13.2	
11^{35}	4480	4.1	30.6	34.8	88
11^{36}	4608	2.3	17.2	19.5	88
(b) The $^1B_2$ state: energy of the 0–0 transition: 34 404 cm^{-1}					
11^{30}	3660	2.4	...	2.4	...
11^{31}	3660	3.5	4.6	8.1	57
11^{32}	3904	4.9	6.5	11.5	57
11^{33}	4026	6.6	8.9	15.5	57
11^{34}	4148	8.4	11.5	19.9	58
11^{35}	4270	10.2	14.3	24.5	58
11^{36}	4392	11.9	16.9	28.8	59
11^{37}	4515	13.2	19.1	32.3	59
11^{38}	4636	14.1	20.7	34.7	59
11^{39}	4758	14.3	21.4	35.6	60
11^{40}	4880	13.9	21.1	35.0	60
11^{41}	5002	12.9	20.0	32.9	61
11^{42}	5124	11.4	18.1	29.5	61
11^{43}	5246	9.7	15.6	25.3	62
11^{44}	5368	7.8	12.9	20.7	62
11^{45}	5490	6.1	10.2	16.2	63
11^{46}	5612	4.5	...	4.5	...

of a very different nature, namely, $\pi\sigma^*$ ($5b_1 14a_1^*$) and $\sigma\pi^*$ ($11b_2 4a_2^*$).

The calculated envelope of the 1^1A_1 state is very complex. Table IV summarises the simplest single overtone vibrations, and a few of the combination modes. All the a_1 modes except modes 5 and 3 occur in the FC analysis, and most of these same vibrations occur in the combination bands. The 1^1A_1 state starts with a two quantum weak vibration, 19^2, a b_1 mode.

TABLE IV. Selected intensities for the Franck-Condon (FC) and Herzberg-Teller (HT) factors for some low-lying singlet states; these are cold bands only, based on harmonic vibration frequencies. In order to allow processing of Herzberg-Teller contributions, the EOM-CCSD were correlated to the TDDFT values, which led to the removal of one imaginary frequency. The frequencies shown here are based upon that correlation. See the supplementary material for additional details.

Vibrational state	Frequency (cm^{-1})	Intensity	
		Franck-Condon	Herzberg-Teller
The $^1A_1$ state: energy of the 0–0 transition: 45 949 cm^{-1}			
0^0	0	75 600	
19^2	142	3 639	
11^1	217	15 810	445
10^1	299	9 737	
9^1	370	5 609	
8^1	495	61 510	1532
7^1	635	33 610	826
6^1	906	5 950	
8^2	990	30 880	804
7^2	1270	10 880	
4^1	1356	46 890	2203
8^3	1385	5 872	
2^1	1608	28 030	1298
1^1	1773	14 830	
4^2	2712	19 750	1632
2^2	3216	6 897	
4^3	4068	4 685	645
$8^1 19^2$	637	2 406	
$8^1 11^1$	712	15 780	465
$8^1 10^1$	794	10 670	
$8^1 9^1$	865	3 499	980
$7^1 11^1$	934	10 510	
$7^1 10^1$	934	6 319	
$9^2 10^1$	1039	3 347	
$7^1 8^1$	1130	38 300	
$8^2 11^1$	1207	4 813	
$7^1 9^2$	1375	11 170	299
$6^1 8^1$	1401	7 590	
$4^1 19^2$	1498	3 411	
$6^1 7^1$	1541	3 773	
$4^1 11^1$	1573	15 330	804
$7^2 9^1$	1640	11 140	
$4^1 10^1$	1655	7 936	
$4^1 9^1$	1726	4 779	
$2^1 11^1$	1825	8 399	440
$4^1 8^1$	1851	55 140	2712
$6^1 8^2$	1896	3 844	
$2^1 10^1$	1907	5 107	
$4^1 7^1$	1991	31 580	1520
$2^1 8^1$	2103	31 460	1528
$7^1 8^3$	2120	3 644	
$1^1 8^1$	2222	11 000	1740
$2^1 7^1$	2243	17 720	850
$4^1 6^1$	2262	5 909	
$4^1 8^2$	2297	15 200	1318
$1^1 7^1$	2359	5 971	938
$2^1 6^1$	2462	3 454	
$2^1 8^2$	2545	13 860	710
$4^1 7^2$	2572	9 932	490
$1^1 8^2$	2763	5 373	895
$2^1 7^2$	2878	5 225	
$4^2 11^1$	2929	6 495	578

TABLE IV. *(Continued.)*

Vibrational state	Frequency (cm^{-1})	Intensity	
		Franck-Condon	Herzberg-Teller
$2^1 4^1$	2964	26 280	2040
$1^1 4^1$	3129	12 420	2694
$4^2 8^1$	3207	21 320	1860
$4^2 7^1$	3347	12 900	1091
$1^1 2^1$	3381	4 635	1007
$2^2 8^1$	3711	6 778	579
$2^2 7^1$	3851	3 946	
$4^2 7^2$	3982	3 933	
$2^1 4^2$	4320	10 710	
$1^1 4^2$	4485	2 927	905
$4^3 8^1$	4563	4 577	673
$2^2 4^1$	4572	6 257	762

The FC modes are predominant, with HT modes making a much smaller contribution. Overall, the FC modes provide an acceptable profile of the VUV band between 43 000 and 49 000 cm^{-1}; however, no single Gaussian band replacement for the stick diagram of Fig. 6 will give the weak structure shown in the experiment. This state is discussed further in relation to attempts to fit the observed profile, in the supplementary material as SM3.

3. The region between 5.8 and 6.5 eV (bands C and D)

For C_6F_5I, a shoulder occurs between bands C and D in the VUV spectra. A similar feature also occurs in the spectrum of C_6F_5H,[35] whereas the same gap in the C_6H_5I VUV spectrum shows a resolved structure.[2] The similarity of the vibrational structure to that of IE_1 for C_6H_5I[2] confirms the presence of the 3s-Rydberg state. The shoulders present in this region for both C_6F_5I and C_6F_5H suggest that the corresponding Rydberg state also occurs there. A summary of the valence states is shown in Table V.

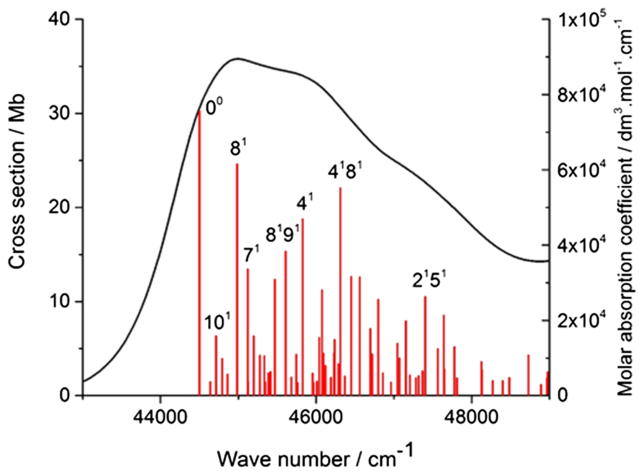

FIG. 6. The principal ππ* (1^1A_1) component of the 45 000 cm^{-1} band for C_6F_5I. The stick spectrum (red) shows the Franck-Condon factor relative line intensities for the simplest vibrational components of the single overtones and combinations of two simultaneously excited modes.

TABLE V. The adiabatic excitation energies for a series of valence singlet states determined by the TDDFT method, and comparison of the corresponding C–I bond lengths.

Energy/eV	Oscillator strength/f(r)	Symmetry	Leading configuration	C–I bond length/Å
5.8603	0.0283	$^1B_2$	$3a_2 7b_1$*	2.075
7.2323	1.0859	$^1A_1$	$3a_2 4a_2$* -$6b_1 7b_1$* - $6b_1 8b_1$*	2.037
7.5923	0.5038	$^1B_2$	$6b_1 4a_2$* + $3a_2 7b_1$*	2.045
8.1663	0.0571	$^1A_1$	$12a_1 13a_1$* + $6b_1 7b_1$*	2.305
8.3063	0.2950	$^1A_1$	$5b_1 8b_1$* + $5b_1 7b_1$*	2.189
8.9423	0.0848	$^1A_1$	$12a_1 13a_1$*	2.072
9.9099	0.4979	$^1A_1$	$6b_1 9b_1$*	2.166

4. The region between 6.5 and 7.5 eV (bands D and E)

These two high oscillator strength bands have been compared previously[4,14,15] with the $^1B_{1u}$ and $^1E_{1u}$ transitions of benzene and are assigned as shown in Table I. The band D (maximum 6.70 eV) is dominated by a $^1A_1$ state, with leading term $3a_2 4a_2$*. The band E (maximum 7.35 eV) is dominated by two states, $^1A_1$ ($5b_1 7b_1$*) and $^1B_2$ ($6b_1 4a_2$*). The C–I bond lengths calculated for these spectrally dominant bands are in the normal range, and FC components dominate.

Many of the observed bands at higher energy are probably Rydberg states, as discussed next.

5. Band F at 7.932 eV (63 977 cm^{-1}) for C_6F_5I

A comparison of the VUV and PES profiles for this region when expanded in a cm^{-1} scale (Fig. 7) shows major similarities in the two spectra, although underlying absorption near 64 500 and 65 250 cm^{-1} occurs in the VUV spectrum. We believe that this overlay of the VUV and PES spectra confirms that the 7.932 eV VUV band is a Rydberg state, rather than the valence state proposed by Eden *et al.*[4] The VUV spectrum of C_6H_5I shows a similar structure for its band F (Fig. 1) at 64 250 cm^{-1} (7.966 eV). Four different Rydberg states (one s, one d, and two f) have been assigned for C_6H_5I in this region, while band F was assigned to a 4d Rydberg state.[1,2] The significant strength of d-Rydberg state cross sections in VUV spectra is often notable, and we associate the 7.932 eV band in C_6F_5I with a 4d-state by analogy. The difference for IE_1 for the two compounds is 4428 cm^{-1} (0.55 eV). We attributed the observed small energy difference in these two 4d states for C_6H_5I and C_6F_5I (273 cm^{-1}, 0.034 eV) to the perfluoro effect. We conclude that in states where ring excitation is predominant, the H and I atoms behave similarly.

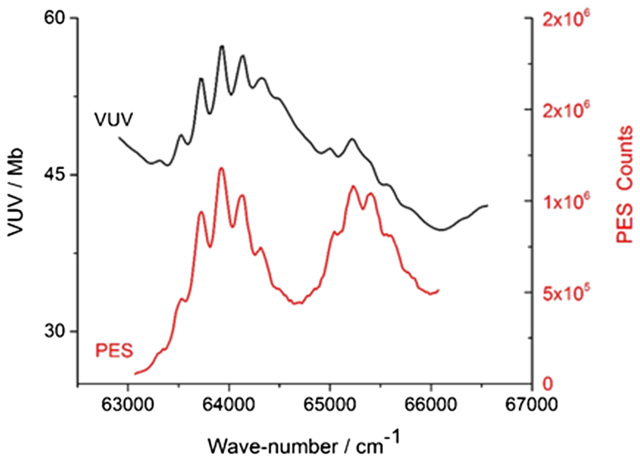

FIG. 7. A comparison of the VUV (black) and PES (red) profiles for the band F at 7.932 eV.

E. Higher Rydberg states observed in the VUV spectrum

The units here are cm^{-1}, and an ionic core based on IE_n is indicated by [n]. The experimental VUV spectrum was simplified by our "subtraction" technique,[1,2,13] to remove broad structures. This enhances the intensity of all states having sharp vibrational features, and the Rydberg states in particular. No data are lost, and any valence states showing fine structure are also amplified.

As a result of assignment of band F (7.932 eV) as a valence state, Eden *et al.*[4] proposed over 50 Rydberg (s, p, d) states based on the four lowest adiabatic ionization energies (AIEs). However, the PES spectra had not been analysed, and we have found that the A state, IE_2, is of $^2A_2$ symmetry.[3] Thus s-Rydberg states in the present VUV spectrum, based on the PES A state, are optically forbidden; the same conclusion arises for other p- and d-Rydberg states, where excitation into an a_1 upper state occurs. This prompted the current investigation, which was assisted by our more highly resolved PES.[3] Small shifts in some AEE relative to the Eden *et al.*[6] occur from the additional accuracy of measurement. Although the fine structure on both X^2B_1 (IE_1) and A^2A_2 (IE_2) allows the AIE to be identified, Rydberg states converging on IE_3 and IE_4 are the easiest to identify; this arises from their separation from other bands and relative intensities in the PES and presence of high 0–0 bands.

We have revised the extensive list of potential Rydberg states given in Tables 3 and 4 of Eden *et al.*[4] in the light of the improved VUV and PES data available here; the results are shown in Tables VI and VII. Our set of assignments account for all of the *clearly distinguishable* peaks in the spectrum, while excluding obvious valence states. Our assignments are broadly in line with what would be expected from the intensities of the bands in the PES and from the n* values of series observed in the other monohalobenzenes.[1,2,36–38] We illustrate our Rydberg assignments for the VUV absorption spectrum of C_6F_5I in Figs. 8 and 9. The separation of the first two peaks in IE_1 of the PES of ~1300 cm^{-1} equates to the separation of the [1]3d state indicated by a starred peak in Fig. 8.

TABLE VI. Comparison of the current and previous assignments of the origin bands of the Rydberg states of C_6F_5I converging on various states of the ion observed in the VUV absorption spectrum. Previous principle quantum numbers are given as valence shell numbering to assist with comparison with our previous studies. Revised previous assignments[4] are marked in red, and several others are omitted as insecure.

T_E/cm^{-1}	T_E/eV	Present assignment	Eden *et al.*[4]
63 925	7.926	[1]3d	Valence band F
66 598	8.257	[1]4p/[3]3p	[1]4p
68 198	8.455	[4]3s	[2]4s
69 489	8.615	[1]4d	-
71 330	8.844	[3]3d	[1]5d
72 063	8.935	[3]3d	[3]3d
72 698	9.013	[4]3p	[1]7s/[2]5s
74 129	9.191	[1]5d	[2]5d
76 071	9.431		
76 919	9.537	[3]4d	[2]7d/[3]6s
77 590	9.620	[3]4d	[2]8d/[3]4d/[4]4s
78 714	9.759		
79 982	9.916	[3]5d	[3]5d
80 226	9.947	[3]5d	[3]6s
80 639	9.998		
81 432	10.096	[3]6d	[3]7s/[3]6d
81 630	10.121	[4]4p	[3]7s/[3]7d
82 916	10.280		
82 329	10.207	[3]7d	[3]7d
83 139	10.308	[4]4d	-
83 566	10.361	[1]nd	
85 122	10.554	[4]4d	-
85 762	10.633	[4]5p	[4]5d
86 246	10.693	[4]5d	[4]6s
86 910	10.775		

F. Comparison of the PES and VUV spectra for C_6H_5I and C_6F_5I

Assignment of the X, A, B, and C states in these PES spectra to the four lowest IEs as $1^2B_1 < 1^2A_2 < 1^2B_2 < 2^2B_1$ are relevant here. However, the appearance of the PES spectra of C_6H_5I and C_6F_5I shows significant differences, owing to differing internal separations from neighbour states. This in turn leads to different levels of vibronic coupling with these neighbours.

Our criterion in determining whether there is an interaction between two adjacent IEs or not is whether the baseline of the PES is re-established between the two states. When overlaps or close spacing occurs in interacting cases, a potential energy curve crossing with the associated conical interaction will be present. This must occur for X^2B_1 and A^2A_2 in C_6F_5I and has been quantified for C_6H_5F.[3] The X and A states in C_6F_5I overlap considerably, whereas those for C_6H_5I are effectively free from interaction. The A and B states overlap very significantly for C_6H_5I, *but weakly for* C_6F_5I. Finally, the C state in both C_6F_5I and C_6H_5I is free-standing.[1] In the non-overlapping cases, the lower energy ionic state, the X^2B_1 state of C_6H_5I, and the B^2B_2 state of C_6F_5I show a significant vibrational structure, which is successfully interpreted in the Franck-Condon factor (FCF) analyses previously discussed.[3] This is less true for the interacting states.

TABLE VII. Transition energies, T_E, and n* values of the origin bands of the Rydberg states of C_6F_5I converging on various states of the ion observed in the VUV absorption spectrum.

			np		nd_1			
State	IE/cm^{-1}	n	TE/cm^{-1}	n*	TE/cm^{-1}	n*	nd_2	n*
X^2B_1	75 858	3			63 925	3.03		
		4	66 598	3.44	69 489	3.45		
		8			74 129	7.97		
A^2A_2	79 525	3	59 260	2.327				
B^2B_2	84 512	3	66 598	2.48	71 330	2.89	72 063	2.97

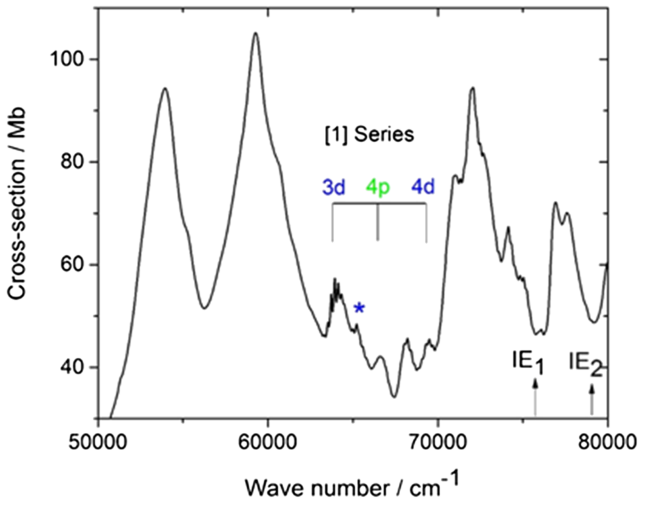

FIG. 8. The low energy region of the Rydberg state studies between 50 000 and 80 000 cm^{-1} (6.199 and 9.919 eV). The revised assignments for the Rydberg series based on the X^2B_1 state (series [1]). See text for *. Very weak structure on the leading edge of the 59 000 cm^{-1} band is the $3a_2X$ state. This is one of the few IE_2 ($^2A_2$) Rydberg excitations with a high calculated cross section, but it is super-imposed on a major valence band.

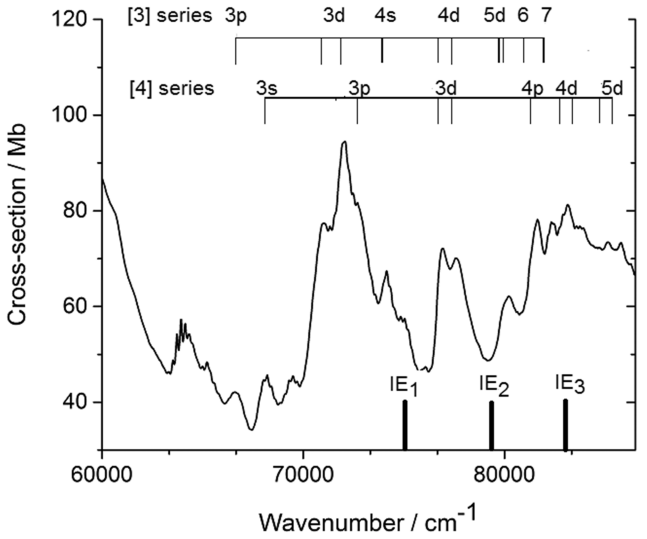

FIG. 9. The VUV absorption between 64 000 and 88 000 cm^{-1} (7.93 and 10.91 eV). Rydberg series based on the B^2B_2 ([3]) and C^2B_1([4]) states. The three lowest IEs are indicated.

IV. CONCLUSIONS

Our recent PES study[3] of C_6F_5I makes a substantial vibrational structure observable for the first time and gives reasonable estimates of two AIEs. The symmetry of the lower ionic states is unambiguous, namely, $X^2B_1 < A^2A_2 < B^2B_2 < C2^2B_1 < D^2A_1 < E3^2B_1$. These rigorous PES assignments show that a number of earlier VUV assignments of Rydberg states[4] cannot be correct, since they are based on optically forbidden states. In addition, the VUV band F, previously assigned to a valence state, now shows a good overlap with the PES footprint of the first ionization energy. Hence the VUV multiplet at 7.932 eV[6] must be a Rydberg state, which we believe is of d-type symmetry. This shifts the energy region, where Rydberg states are assigned, and leads to a number of assignment changes.

Our "subtraction" technique[1–3] allows more certain identification of a weak VUV structure to be assigned to Rydberg states. The whole profile is now consistent with C_6H_5I and hence with the other members of the C_6H_5X (X = F, Cl, and Br) series.[1,2,33–35] There is a correlation between several of the Rydberg state excitation energies between the C_6H_5I and C_6F_5I series, with an energy difference close to 4775 cm^{-1} for the replacement of 5H × 5F in the molecules. Such a value is more consistent with the excitation of a π-electron MO than a σ-MO, where the effect would be expected to be larger.

We have considered vibronic interactions in some detail. Both Franck-Condon and Herzberg-Teller contributions were determined for the lowest group of UV+VUV absorptions. The onset of the UV absorption region contains two very weak singlet states of $^1B_1$ and $^1B_2$ symmetries. These two states involve excitation from a π-MO and σ-MO into a C–I antibonding σ*-orbital of a_1 symmetry; this leads to major lengthening of the C–I bond relative to the ground state. The experimental 0–0 bands are very weak and poorly defined. The calculated FC profiles support these assignments, while the $^1B_1$ state at the spectral onset is dominated by Herzberg-Teller contributions to the intensity, with progressively less HT for the next two higher states.

The main benzene-like UV band lying between 5.1 and 6 eV, although dominated by a $^1A_1$ (ππ*) excitation, is far from simple. Three allowed states lie under the envelope, with sharply differing oscillator strengths, $^1A_1 \gg 2^1B_2$ (ππ*) $> 2^1B_1$ (πσ*). The weak structure observed bears a reasonable relationship to the predicted FC profile for an isolated $^1A_1$ state at this energy.

The most intense bands in the VUV spectrum are band D (maximum 6.70 eV) is dominated by the $^1A_1$ state, with leading term $3a_24a_2$*, and band E (maximum 7.35 eV) dominated by two states, $^1A_1$ ($5b_17b_1$*) and $^1B_2$ ($6b_14a_2$*).

SUPPLEMENTARY MATERIAL

See supplementary material for SM1—The MRD-CI of C_6F_5I showing a list of singlet state energies, oscillator strengths, and second moments of the charge distribution. Table SM1—The MRD-CI study of C_6F_5I showing singlet state energies, oscillator strengths, and second moments of the charge distribution. Figure SM1—Comparison of the molecular structures of the lower excited states with the partially oriented NMR structure. SM2—Structures of the ground and other singlet states of C_6F_5I using both EOM-CCSD and TDDFT methods. Table SM2—A comparison of the EOM-CCSD structures for C_6H_5I and C_6F_5I. SM3—More detailed discussion of band C. SM4—Correlation of the EOM-CCSD and TDDFT harmonic frequency calculations.

ACKNOWLEDGMENTS

We thank the following people and institutions for support: ASTRID2 facility for grants to carry out the VUV absorption study. NSCCS super-computing facility of the UK for support. The Italian MIUR Project (No. PON01-01078/8). Professor Vincenzo Barone and Dr. Julien Bloino for helpful discussions. C. Puglia (Uppsala University, Sweden) and the Carl Tygger Foundation for making available the VG-Scienta SES-200 photoelectron analyser at the Gas Phase beamline, Elettra, Italy.

[1] M. H. Palmer, T. Ridley, S. V. Hoffmann, N. C. Jones, M. Coreno, M. de Simone, C. Grazioli, M. Biczysko, A. Baiardi, and P. Limão-Vieira, J. Chem. Phys. **142**, 134302 (2015).
[2] M. H. Palmer, T. Ridley, S. V. Hoffmann, N. C. Jones, M. Coreno, M. de Simone, C. Grazioli, M. Biczysko, and A. Baiardi, J. Chem. Phys. **142**, 134301 (2015).
[3] M. H. Palmer, M. Coreno, M. de Simone, S. V. Hoffmann, N. C. Jones, C. Grazioli, A. Baiardi, T. Zhang, K. A. Peterson, and M. Biczysko, J. Chem. Phys. **146**, 084302 (2017).
[4] S. Eden, M.-J. Hubin-Franskin, J. Delwiche, S. V. Hoffmann, N. J. Mason, and N. C. Jones, Chem. Phys. **359**, 111 (2009).
[5] V. Barone, J. Bloino, and M. Biczysko, Vibrationally-resolved electronic spectra in GAUSSIAN 09, Revision A.02, Gaussian, Inc., 2009, see http://dreamslab.sns.it, accessed April 01, 2016.
[6] J. Bloino, M. Biczysko, O. Crescenzi, and V. Barone, J. Chem. Phys. **128**, 244105 (2008).
[7] V. Barone, J. Bloino, M. Biczysko, and F. Santoro, J. Chem. Theory Comput. **5**, 540 (2009).
[8] J. Bloino, M. Biczysko, F. Santoro, and V. Barone, J. Chem. Theory Comput. **6**, 1256 (2010).
[9] V. Barone, M. Biczysko, and J. Bloino, Phys. Chem. Chem. Phys. **16**, 1759 (2014).
[10] M. B. Robin, *Higher Excited States of Polyatomic Molecules* (Academic Press, 1985), Vol. III, p. 362.
[11] A. P. Hitchcock, P. Fischer, A. Cedanken, and M. B. Robin, J. Phys. Chem. **91**, 531 (1987).
[12] K. Kavita and P. K. Das, J. Chem. Phys. **117**, 2038 (2002).
[13] J. A. Griffiths, K.-W. Jung, and M. A. El-Sayed, J. Phys. Chem. **100**, 7989 (1996).
[14] J. E. Freitas, H. Jin Hwang, and M. A. El-Sayed, J. Phys. Chem. **97**, 12481 (1993).
[15] D. Ajitha, D. G. Fedorov, J. P. Finley, and K. Hirao, J. Chem. Phys. **117**, 7068 (2002).
[16] D. Murdock, M. B. Crow, G. A. D. Ritchie, and M. N. R. Ashfold, J. Chem. Phys. **136**, 124313 (2012).
[17] J. F. Stanton and J. Gauss, J. Chem. Phys. **101**, 8938 (1994).
[18] R. Bauernschmitt and R. Ahlrichs, Chem. Phys. Lett. **256**, 454 (1996).
[19] R. J. Buenker and S. Krebs, in *Recent Advances in Multireference Methods*, edited by K. Hirao (World Scientific, Singapore, 1999), pp. 1–29.
[20] CFOUR, Coupled-cluster techniques for computational chemistry, a quantum-chemical program package by J. F. Stanton, J. Gauss, M. E. Harding, and P. G. Szalay with contributions from A. A. Auer, R. J. Bartlett, U. Benedikt, C. Berger, D. E. Bernholdt, Y. J. Bomble, L. Cheng, O. Christiansen, M. Heckert, O. Heun, C. Huber, T.-C. Jagau, D. Jonsson, J. Juselius, K. Klein, W. J. Lauderdale, F. Lipparini, D. A. Matthews, T. Metzroth, L. A. Muck, D. P. O'Neill, D. R. Price, E. Prochnow, C. Puzzarini, K. Ruud, F. Schiffmann, W. Schwalbach, C. Simmons,

S. Stopkowicz, A. Tajti, J. Vazquez, F. Wang, and J. D. Watts, and the integral packages MOLECULE (J. Almlof and P. R. Taylor), PROPS (P. R. Taylor), ABACUS (T. Helgaker, H. J. A. Jensen, P. Jorgensen, and J. Olsen), and ECP routines by A. V. Mitin and C. van Wullen, for the current version, 2010, see http://www.cfour.de.

[21] J. F. Stanton and R. J. Bartlett, J. Chem. Phys. **98**, 7029 (1993).

[22] M. J. Frisch, G. W. Trucks, H. B. Schlegel, G. E. Scuseria, M. A. Robb, J. R. Cheeseman, G. Scalmani, V. Barone, B. Mennucci, G. A. Petersson, H. Nakatsuji, M. Caricato, X. Li, H. P. Hratchian, A. F. Izmaylov, J. Bloino, G. Zheng, J. L. Sonnenberg, M. Hada, M. Ehara, K. Toyota, R. Fukuda, J. Hasegawa, M. Ishida, T. Nakajima, Y. Honda, O. Kitao, H. Nakai, T. Vreven, J. A. Montgomery, Jr., J. E. Peralta, F. Ogliaro, M. Bearpark, J. J. Heyd, E. Brothers, K. N. Kudin, V. N. Staroverov, T. Keith, R. Kobayashi, J. Normand, K. Raghavachari, A. Rendell, J. C. Burant, S. S. Iyengar, J. Tomasi, M. Cossi, N. Rega, J. M. Millam, M. Klene, J. E. Knox, J. B. Cross, V. Bakken, C. Adamo, J. Jaramillo, R. Gomperts, R. E. Stratmann, O. Yazyev, A. J. Austin, R. Cammi, C. Pomelli, J. W. Ochterski, R. L. Martin, K. Morokuma, V. G. Zakrzewski, G. A. Voth, P. Salvador, J. J. Dannenberg, S. Dapprich, A. D. Daniels, O. Farkas, J. B. Foresman, J. V. Ortiz, J. Cioslowski, and D. J. Fox, GAUSSIAN 09, Revision D.01, Gaussian, Inc., Wallingford, CT, 2013.

[23] M. F. Guest, I. J. Bush, H. J. J. Van Dam, P. Sherwood, J. M. H. Thomas, J. H. Van Lenthe, R. W. A. Havenith, and J. Kendrick, Mol. Phys. **103**, 719 (2005).

[24] T. H. Dunning, J. Chem. Phys. **90**, 1007 (1989); R. A. Kendall, T. H. Dunning, Jr., and R. J. Harrison, J. Chem. Phys. **96**, 6796 (1992).

[25] K. A. Peterson, D. Figgen, E. Goll, H. Stoll, and M. Dolg, J. Chem. Phys. **119**, 11113 (2003).

[26] T. H. Dunning and P. J. Hay, in *Methods of Electronic Structure Theory*, edited by H. F. Schaefer III (Plenum Press, 1977), Vol. 2.

[27] L. E. Roy, P. J. Hay, and R. L. Martin, J. Chem. Theory Comput. **4**, 1029 (2008).

[28] P. J. Hay and W. R. Wadt, J. Chem. Phys. **82**, 270 (1985).

[29] A. D. Becke, J. Chem. Phys. **98**, 5648 (1993).

[30] A. Haloui and E. Haloui, Magn. Reson. Chem. **49**, 717 (2011).

[31] P. Pyykko and M. Atsumi, Chem. Eur. J. **15**, 186 (2009).

[32] P. Pyykko and M. Atsumi, Chem. Eur. J. **15**, 12770 (2009).

[33] J. Philis, A. Bolovinos, G. Andritsopoulos, E. Pantos, and P. Tsekeris, J. Phys. B: At. Mol. Phys. **14**, 3621 (1981).

[34] H. H. Jaffé and M. Orchin, *Theory and Applications of Ultraviolet Spectroscopy* (Wiley, New York, 1962), Chap. 12.2, p. 247.

[35] T. Ridley, D. M. Rogers, and K. P. Lawley, J. Chem. Phys. **141**, 154310 (2014).

[36] M. H. Palmer, T. Ridley, S. V. Hoffmann, N. C. Jones, M. Correno, M. de Simone, C. Grazioli, T. Zhang, M. Biczysko, A. Baiardi, and K. A. Peterson, J. Chem. Phys. **144**, 204305 (2016).

[37] M. H. Palmer, T. Ridley, S. V. Hoffmann, N. C. Jones, M. Coreno, M. de Simone, C. Grazioli, T. Zhang, M. Biczysko, A. Baiardi, and K. Peterson, J. Chem. Phys. **143**, 164303 (2015).

[38] M. H. Palmer, T. Ridley, S. V. Hoffmann, N. C. Jones, M. Coreno, M. de Simone, C. Grazioli, T. Zhang, M. Biczysko, A. Baiardi, and K. A. Peterson, J. Chem. Phys. **144**, 124302 (2016).